Electronic and acoustic-phonon inter-Landau-level Raman scattering in $GaAs/Al_xGa_{1-x}As$ multiple quantum wells

A. Fainstein, T. Ruf, and M. Cardona
Max-Planck-Institut für Festkörperforschung, Heisenbergstrasse 1, 70569 Stuttgart, Germany

V. I. Belitsky and A. Cantarero
Departamento de Física Aplicada, Universidad de Valencia, Burjasot, E-46100 Valencia, Spain
(Received 31 October 1994)

We present an experimental study of inter-Landau-level excitations in undoped $GaAs/Al_xGa_{1-x}As$ multiple quantum wells in high magnetic fields by means of Raman scattering. The experiments were performed in Faraday backscattering geometry with the field along the growth axis, using circularly polarized light for resonant excitation of low-index magneto-optical transitions between Landau levels. We observe two types of peaks. One of them, present in both Stokes and anti-Stokes regions at a constant Raman shift, corresponds to the electron cyclotron energy. We attribute it to electronic Raman scattering from a quasistationary population of photoexcited carriers. To account for the observation of these lines, which are forbidden in backscattering geometry, we present a theory of electronic Raman scattering that includes the effect of interface roughness. Such roughness allows Landau-number nonconserving steps and makes cyclotron energy scattering of electrons possible. Another type of structure occurs at the energy of magneto-optical interband transitions close to the exciting laser and is due to coherent acoustic-phonon emission processes. The breakdown of crystal momentum conservation along the growth axis due to layer thickness fluctuations leads to scattering by phonons from the whole Brillouin zone. We discuss possible acoustic-phonon scattering mechanisms and show that two-phonon emission causes triple resonances, which are responsible for the luminescencelike peaks observed at interband magneto-optical transition energies. The observation of cyclotron scattering in resonant Raman experiments leads to a way of determining electronic masses in undoped quantum well structures.

I. INTRODUCTION

Phonons and inter-Landau-level electronic transitions constitute the lower energy excitations of semiconductor multiple quantum well (MQW) structures when the electronic levels are fully quantized by a strong magnetic field applied along the growth axis z.[1] These excitations can be most conveniently studied by Raman scattering.[1]

Raman spectra of MQW's and superlattices usually exhibit characteristic folded phonon doublets.[1] In addition to these sharp lines, acoustic modes from the whole Brillouin zone have been shown to contribute to a continuous Raman emission background with intensity anomalies at the dispersion gaps.[2,3] This background appears in MQW's for which layer thickness fluctuations, i.e., disorder, cause a partial breakdown of crystal momentum conservation along the growth direction (q_z).[2] Also, structures in the Raman spectra observed at the anticrossings of longitudinal and transverse acoustic branches have been explained[3] as being due to interface-roughness-mediated scattering by phonons with nonvanishing in-plane wave vector component $q_\perp$. A theory of disorder-induced acoustic-phonon Raman scattering, both with and without applied magnetic field, was presented in Ref. 4. In this theory, only *intra*-Landau-level scattering was considered. Therefore, the Landau-level electronic structure is not of central importance, the main effect of the magnetic field being to provide additional confinement and thus an enhancement of the Raman intensity.

Electronic *inter*-Landau-level scattering has been reported for two-dimensional electron gases in modulation doped GaAs/(AlGa)As MQW's.[5] Such Landau-level excitations were also studied in nominally undoped quantum well structures, where low concentrations of carriers were achieved by photoexcitation.[6] In this latter case, and consistent with the selection rules, electron cyclotron energy scattering was *not* observed in Faraday geometry with the magnetic field along z, but only for tilted magnetic fields where coupled intersubband-Landau-level excitations are allowed.

In this paper we present an experimental study of inelastic light scattering in *nominally undoped* $GaAs/Al_xGa_{1-x}As$ MQW's in high magnetic fields, with Raman spectra excited resonantly at interband transitions between low-index ($n \leq 5$) heavy-hole to electron Landau levels. The experiments were performed in backscattering Faraday geometry with the field applied along the growth axis. We focus our attention on the energy region of electron inter-Landau-level scattering. Besides the luminescence from thermalized carriers[7,8] and the above described acoustic-phonon continuous emission background, other strong emission structures occur in this energy range: Raman scattering peaks are observed which are related to both electronic and acoustic-phonon

processes. The former show up in the Stokes as well as in the anti-Stokes region of the spectra. Their Raman shifts are equal to the cyclotron energy of conduction electrons. The latter appear as strong peaks close to the exciting laser frequency and correspond to the energy of interband magneto-optical transitions between valence Landau states derived from the first heavy-hole mass subband and conduction electron states (e-hh).

We present a theory of electronic Raman scattering that assumes a quasistationary concentration of hot photoexcited electrons and includes the effect of disorder. Disorder, as due to interface roughness or impurities, allows Landau number nonconserving steps and makes cyclotron energy scattering of electrons possible. The peaks observed at Raman shifts equal to the cyclotron energy are well accounted for by the theory which, in addition, predicts the appearance of other side features when the broadening of final states is included. To explain the emission peaks observed at photon frequencies of conduction to valence Landau-level transitions we also discuss qualitatively one-phonon, one-phonon plus roughness, and two-phonon scattering mechanisms.

Our observations enable us to experimentally separate electron and hole contributions of magneto-optical transitions and hence allow us to determine electron effective masses in undoped MQW's. We compare our results with previous theoretical and experimental determinations of electron effective masses in MQW's.

The paper is organized as follows. In Sec. II we present the experimental results. Section III is devoted to the theory of disorder-induced electronic Raman scattering and acoustic-phonon scattering, as well as the analysis of our results. Conclusions are presented in Sec. IV.

II. EXPERIMENT

Our results were obtained for a MQW composed of 40 periods of 100-Å GaAs wells separated by 103-Å $Al_{0.35}Ga_{0.65}As$ barriers. This sample has been used previously for the study of the acoustic-phonon continuous emission background.[2] Also, a magneto-optical study of its electronic structure was made and will be presented in Ref. 9. The experiments were carried out in magnetic fields up to 14 T in backscattering Faraday geometry, with the propagation of incident and scattered light normal to the (001) plane and parallel to the magnetic field. The spectra were taken with circularly polarized photons. As usual, we describe the polarization configuration in the notation $\overline{z}(\sigma^{\eta},\sigma^{\lambda})z$, where $\eta,\lambda=\pm$ indicate the circular polarization of the exciting or scattered light, respectively. All results were obtained at 10 K, with the excitation power kept purposely low, at about 5 W cm^{-2}, in order to prevent the buildup of a large photoexcited electron population.

Figure 1 shows a typical luminescence spectrum obtained by resonantly exciting the e-hh magneto-optical interband transition with Landau quantum number $n=3$ (hereafter denoted as LLn). We define three energy regions. (i) The range of strong QW edge luminescence around 1.55 eV is followed by a high energy tail where

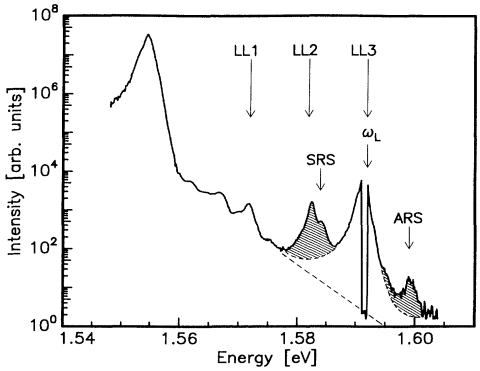

FIG. 1. Luminescence spectrum of a 100-Å-well, 103-Å-barrier GaAs/$Al_{0.36}Ga_{0.64}As$ MQW taken at 4.7 T in resonance with LL3, in $\overline{z}(\sigma^{-},\sigma^{-})z$ Faraday backscattering geometry. Besides the incoherent luminescence tail and the acoustic-phonon emission background (dashed line), other peaks are observed in Stokes and anti-Stokes regions at energy shifts of the order of the cyclotron energy (shaded regions).

peaks at interband magneto-optical transitions which originate in the singular density of states at Landau levels are observed. This tail comes from the recombination of thermalized electrons with a temperature somewhat larger than the lattice temperature. It hence follows a Maxwellian energy distribution (linear in a log scale).[10] The study of the positions of these luminescence peak vs magnetic field enables one to draw fan plots of magneto-optical transitions.[7,11] (ii) In the range within 5 meV of the exciting laser (ω_l) the continuous emission background described in Refs. 2–4 is observed. This feature decays strongly away from the laser energy. It arises from emission of acoustic phonons in Raman processes without conservation of the quasimomentum component q_z. (iii) Finally, there is a range of energies where peaks due to inter-Landau-level scattering, considered in this work, are observed (shaded regions in Fig. 1).

We discuss first the peak labeled LL2 in the "inter-Landau-level scattering energy region" of Fig. 1, i.e., the e-hh magneto-optical transitions LLn closest to the excitation energy. This peak distinguishes itself from the other lower energy ones also due to e-hh Landau level transitions, in several ways. First, as shown in Fig. 1, its amplitude is larger than that expected for the high energy tail of the luminescence. Second, while the intensity of the lower frequency peaks has approximately a quadratic dependence on excitation power, peaks like LL2 exhibit a linear behavior. Third, we find a characteristic polarization dependence. The spectrum shown in Fig. 1 was obtained in $\overline{z}(\sigma^{-},\sigma^{-})z$ geometry. An enhanced LLn peak close to the laser line appears also for $\overline{z}(\sigma^{+},\sigma^{+})z$ polarization. However, for crossed polarizations $\overline{z}(\sigma^{\pm},\sigma^{\mp})z$, strong peaks close to the laser line are absent and the whole high energy part of the spectra has approximately a Maxwellian energy dependence.

The polarization and power dependence of LL2 described above is similar to that reported for the continuous background attributed to acoustic phonons,[2] thus indicating that both features may have the same origin. We

therefore suggest that LL2 is also due to Raman scattering involving acoustic phonons. The coherent character of such scattering is in contrast to the incoherent luminescence from thermalized electrons and holes, which are responsible for the high energy Maxwellian tail on which LL2 is superimposed.

The Raman scattering nature of LL2 in Fig. 1 is also revealed by its resonance behavior. In Fig. 2(a) we present magneto-oscillation profiles measured by choosing an exciting laser energy (ω_l), setting the spectrometer to the Raman shift of interest ($\Delta = \omega_l - \omega_s$) with a spectral bandpass of 0.3 cm^{-1} width, and recording the scattered light intensity (ω_s) vs magnetic field. The laser energy at which the intensity profiles were measured is indicated by the horizontal dashed line in Fig. 2(b), where a schematic fan plot[9] of the e-hh transitions studied is shown. The observed maxima are attributed to resonances with magneto-optical transitions between valence hole and conduction electron Landau levels. Around 6 T, resonances of *incoming* (fixed field) and *outgoing* character (resonance field dependent on Δ, marked with asterisks) are observed. A strong enhancement occurs at $\Delta = 86$ cm^{-1} when incoming and outgoing resonances coincide and a double-resonance condition is fulfilled. For the different interband transitions, double resonances are indicated with vertical arrows in Fig. 2(b). Note that these resonances involve transitions with different Landau states for both electrons and holes, e.g., LL3 in the incoming and LL2 in the outgoing channel.

The resonance behavior can also be analyzed by studying Raman spectra for different laser energies. In Fig. 3 we present a series of spectra taken at 4.7 T above and below incoming resonance with LL3 ($\omega_l = 1.5916$ eV). For ω_l close to resonance, the intensity of LL2 is larger than that of LL1. This relation is reversed for spectra excited far away from resonance. In the latter case, the intensity ratio approaches the expected Maxwellian distribution. The LLn peaks coincide with magneto-optical transitions and thus can be labeled as "outgoing" resonances.[11] The strong increase in the intensity of LL2 for "incoming" resonant excitation at LL3, revealed in the spectra of Fig. 3, indicates correspondingly a double-resonance process.

We note that the "Raman shift" of LL2 in Fig. 3 depends on excitation energy. In fact, the emission frequency is "fixed" to the MQW Landau levels, thus resembling a luminescence process.[7,11] As described above, and justified theoretically in Sec. III, it is the polarization, resonance behavior, and dependence on laser power that leads us to label this line as a Raman-type scattering processes.

We next turn our attention to the other peaks observed in the shaded regions of Fig. 1 and labeled SRS and ARS (Stokes-Raman and anti-Stokes Raman scattering) in Figs. 1 and 3. Contrary to the previously described LL2 feature, both the SRS and ARS peaks have constant Raman shifts for different laser energies, i.e., they are "standard" Raman lines. These peaks are strongly resonant and cannot be observed away from resonance with LLn transitions.

The most important signature of SRS and ARS is their magnetic-field dependence. In Fig. 4 we show the Raman shift of the SRS and LLn signals as a function of the applied magnetic field for spectra obtained at a fixed excitation energy [dashed line in Fig. 2(b)]. The shift of the LLn features decreases as the field increases, corresponding to the fact that the magneto-optical transitions approach the laser frequency. On the other hand, the Raman shift of SRS increases linearly with increasing field. We find that it corresponds to the cyclotron energy of the electrons, as calculated by fitting the magneto-optical transitions using a Luttinger Hamiltonian.[9] This suggests that the observed peaks (SRS and ARS) are due to electronic inter-Landau-level excitations. Correspondingly, the difference between the separation of successive

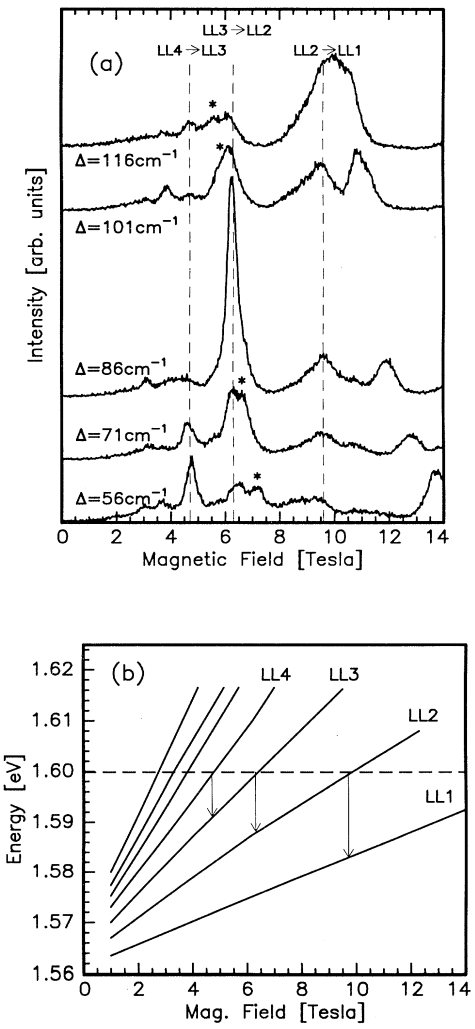

FIG. 2. (a) Magneto-oscillation profiles measured with exciting laser at 1.5999 eV (at resonance with LL4 at 4.7 T) in $\bar{z}(\sigma^-,\sigma^-)z$ configuration. Resonances of incoming (dashed vertical lines) and outgoing (asterisks) character can be distinguished. A strong enhancement is observed when the two types of resonances coincide and a double resonance condition is met. (b) Fan plot of the e-hh magneto-optical transitions for the configuration studied; the horizontal line indicates the laser energy and the vertical arrows the doubly resonant inter-Landau-level processes studied.

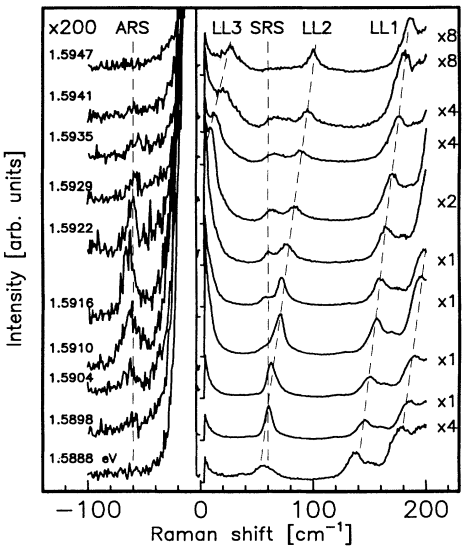

FIG. 3. Raman spectra taken at 4.7 T, around resonant excitation with the LL3 interband magneto-optical transition (1.5916 eV), in $\bar{z}(\sigma^-,\sigma^-)z$ configuration. Two types of peaks can be distinguished according to the dependence of their "Raman shifts" on excitation energy: those at energies fixed to e-hh transitions (LLn) and "true" Raman features in Stokes and anti-Stokes regions (SRS and ARS). Both the Raman features and the LLn peak closest to the laser are strongly resonant.

lines in the fan plot of magneto-optical transitions and the SRS (ASR) Raman shift gives the hole contribution to the cyclotron energy.

We find some selection rules for these features, although not as stringent as those observed for the resonant LLn peaks. The SRS and ARS peaks appear in both parallel and crossed polarizations with about three times larger intensity in the parallel geometry.

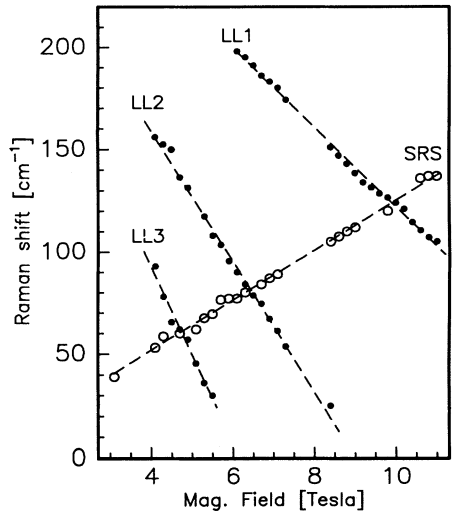

FIG. 4. Magnetic field dependence of Raman shifts for LLn and SRS peaks, obtained with the laser at 1.5999 eV in $\bar{z}(\sigma^-,\sigma^-)z$ configuration. The former correspond to interband e-hh magneto-optical transitions. The energy of the latter increases with applied field and is equal to the cyclotron energy of conduction electrons.

III. THEORY AND DISCUSSION

A. Electronic Raman scattering

We now address the question of the microscopic scattering mechanism for the above described SRS and ARS features. The excitation of one electron cyclotron quantum in an electronic Raman process may result from the two-step sequence of events shown schematically in Fig. 5(a):[12] In the first step, an electron is optically excited from the valence band to an intermediate Landau level in the conduction band and, in the second step, an electron that was *previously* in a Landau level below (Stokes) or above (anti-Stokes) the excited one recombines with the hole in the valence band. In order to describe our observations in a nominally undoped MQW by such a mechanism, we have to assume that a quasistationary concentration of electrons is created by the exciting laser. The observed luminescence tail supports this assumption. The corresponding Feynman diagram for the Raman efficiency is shown in Fig. 5(b).[13–15] The notation for the electron and hole states is the same as that used in Ref. 2. N indicates the size-quantized subband, n,m,p,l are Landau numbers, and k_y is the wave vector (i.e., crystal momentum) in the y direction. The frequency and the in-plane crystal momentum variables

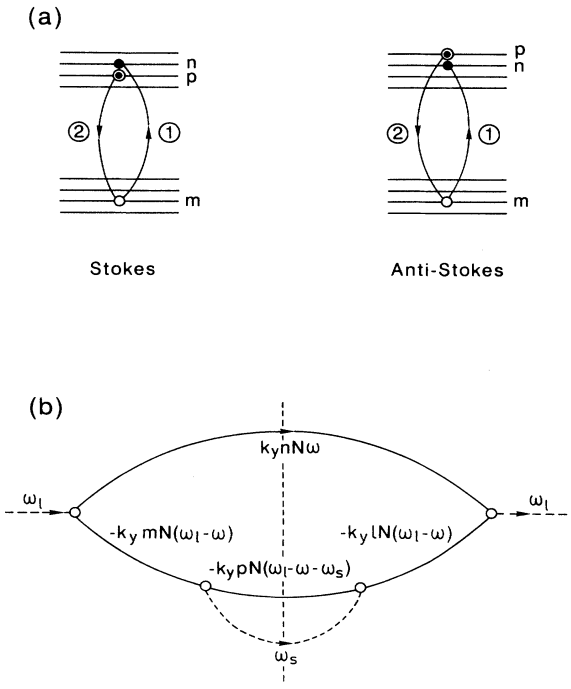

FIG. 5. (a) Schematic representation of the electronic Raman scattering process via single-particle inter-Landau-level excitations. (b) Feynman-type diagram for the scattering efficiency. The vertical dashed line indicates the final state in the scattering process.

are taken such that they are conserved in all vertices of interaction with light. The middle section of the diagram in Fig. 5(b) (dashed vertical line) corresponds to the final state in the scattering process, which includes a quantum of scattered radiation and an electron and a hole in the electronic Landau levels n and p, respectively.

Note that, in the general process described by the diagram of Fig. 5(b), we have taken the Landau numbers of all intermediate states to be different. This in fact is not realistic for two reasons. (i) In the backscattering geometry the in-plane wave vectors of the laser and scattered light are zero. Hence the matrix elements for interaction with light impose the condition $n = m = p = l$. For instance, the two vertices of interaction with the incident light in Fig. 5(b) results in a factor proportional to

$$f_{n,m}(x) = \frac{\min(n!, m!)}{\max(n!, m!)} \times \exp(-x) x^{|n-m|} \left[L^{|n-m|}_{\min(n,m)}(x) \right]^2, \quad (1)$$

where $x = l_H^2 \kappa_{l\perp}^2/2$, $l_H = \sqrt{\hbar c/eH}$ is the magnetic length, $\kappa_{l\perp}$ is the in-plane momentum of light, and $L^{|n-m|}_{\min(n,m)}(x)$ are Laguerre polynomials. Equation (1) vanishes for $n \neq m$ and $\kappa_{l\perp} = 0$. (ii) Even for an arbitrary direction of incident light and thus nonvanishing $\kappa_{l\perp}$, the value $l_H \kappa_{l\perp} \ll 1$ and $f_{n,m}(x)$ is negligibly small.

One possible way to overcome the problem of Landau number conservation in backscattering is, as discussed below, to consider a fourth-order process which also includes scattering by interface roughness. Nevertheless, and in order to discuss the physical processes involved in the scattering mechanism considered, we give first an expression for the Raman efficiency assuming a Landau-number-nonconserving interaction with light. Such nonconservation is possible when the longitudinal and transverse motions of carriers with respect to the magnetic field cannot be separated, as assumed to derive Eq. (1). This may result from terms linear, cubic, or fourth order in $\vec{k}$ in the bulk electronic bands. *Neglecting the broadening of final states*, we find the scattering efficiency

$$\frac{dS}{d\omega_s} \propto \frac{\delta(\omega_l - \omega_s - (n-p)\omega_e)}{\left[\Omega_N - \left(n+\frac{1}{2}\right)\omega_e - \left(m+\frac{1}{2}\right)\omega_h\right]^2 + \gamma_{h,m}^2}, \quad (2)$$

where

$$\Omega_N = \omega_l - E_g - E_N^e - E_N^h \quad (3)$$

and the indices (h, m) represent a hole in the valence subband with Landau number m. In Eq. (2), the distribution functions of electrons n_e^c and n_e^v also have to be included. They lead for the first transition of Fig. 5(a) to the factor $n_e^v(m, N)[1 - n_e^c(n, N)]$ and for the second one to $n_e^c(p, N)$. We hence note that the dependence of the Raman efficiency on the excitation energy ω_l may be influenced not only by the resonant denominator of Eq. (2), but also by the electron and hole distribution functions.

It follows from Eq. (2) that peaks in the Raman spectra are expected at the scattered frequency $\omega_s = \omega_l - (n-p)\omega_e$ provided $n_e^c(p, N) \neq 0$. According to Eq. (1), the main contribution to one-cyclotron energy scattering ($\omega_s = \omega_l \pm \omega_e$) comes, after summing over n, p, m as implied by the diagram in Fig. 5(b), from (i) $n = m = p \pm 1$ and (ii) $n = m \pm 1 = p \pm 1$, with the + (−) sign for Stokes (anti-Stokes) processes.

The above result follows from the diagram in Fig. 5(b) only if we neglect the broadening of the final states, i.e., that of the electron in Landau level n and the hole in Landau level p. We show next that a nonzero broadening of these final states generates further interesting features. The discussion here is an extension of the theory given in Ref. 16 for single-particle intersubband electronic excitations in quantum wells. In order to include the broadening of *final* states we have to replace Eq. (2) by

$$\frac{dS}{d\omega_s} \sim \frac{1}{\gamma_{h,n}} \frac{F(\Omega_{nN}, \Delta, \gamma_{h,i}, \gamma_{e,j})}{[\Omega_{nN}^2 + (\gamma_{e,n} + \gamma_{h,n})^2]\,[(\Delta - \omega_e)^2 + (\gamma_{e,n} + \gamma_{e,n-1})^2]\,[(\Delta - \Omega_{nN} - \omega_e)^2 + (\gamma_{e,n-1} + \gamma_{h,n})^2]}, \quad (4)$$

where

$$\begin{aligned} F(\Omega_{nN}, \Delta, \gamma_{h,i}, \gamma_{e,j}) = {} & \gamma_{e,n-1}\gamma_{h,n}(\Delta - \Omega_{nN} - \omega_e)^2 + \gamma_{e,n}\gamma_{e,n-1}(\Delta - \omega_e)^2 + \gamma_{e,n}\gamma_{h,n}\Omega_{nN}^2 \\ & + \gamma_{e,n}^3(\gamma_{e,n-1} + \gamma_{h,n}) + \gamma_{e,n-1}^3(\gamma_{e,n} + \gamma_{h,n}) + \gamma_{h,n}^3(\gamma_{e,n} + \gamma_{e,n-1}) \\ & + 2(\gamma_{e,n}\gamma_{e,n-1} + \gamma_{e,n}\gamma_{h,n} + \gamma_{e,n-1}\gamma_{h,n})^2. \end{aligned} \quad (5)$$

Equation (4) corresponds to case (i) above: $n = m = p + 1$, with $\Omega_{nN} = \Omega_N - (n + 1/2)\omega_\mu = \omega_l - E_{\mathrm{LL}n}$, $\omega_\mu = \omega_e + \omega_h$, and $\Delta = \omega_l - \omega_s$.

For $\gamma_{e,n}, \gamma_{e,n-1} \to 0$, Eq. (4) reproduces the result of Eq. (2), namely, a sharp peak at $\omega_s = \omega_l - \omega_e$. For the general case $\gamma_{e,n} \neq 0$, Eq. (4) leads for $\Omega_{nN} = 0$, i.e., $\omega_l = E_{\mathrm{LL}n}$ (incoming resonance), to a similar Raman spectrum, broadened by the full width at half maximum $\gamma_{e,n} + \gamma_{e,n-1}$ and strongly resonance enhanced. Note that the peak of this Raman spectrum, at $\Delta = \omega_e$, corresponds also to outgoing resonance ($\omega_s = \omega_l - \omega_e$): In this case one can thus speak of a *double resonance* for SRS. If we detune the incoming resonance ($\Omega_{nN} \neq 0$), however, two peaks appear in the Raman spectrum which therefore differs strongly from a Lorentzian: One appears for $\Delta = \omega_e$ [second resonant denominator in Eq. (4)], the other (third resonant denominator) for $\omega_s = E_g + E_N^e + E_N^h + (n + 1/2)\omega_\mu - \omega_e = E_{\mathrm{LL}n} - \omega_e$,

which corresponds to an outgoing resonance absent in Eq. (2). The ω_s of this second feature is thus independent of laser frequency. Hence, in spite of being a Raman process, it behaves like luminescence. From Eq. (5) we note that this characteristic frequency appears whenever the broadening of the first photoexcited state $\gamma_{e,n} \neq 0$, even when that of the recombining electron state is zero.

The physical origin of the above described resonances can be clarified by considering the two-step process schematized in Fig. 5. Let us first discuss the situation in which no broadening is included. When the excitation is detuned with respect to $E_{\mathrm{LL}n}$ ($\Omega_{nN} \neq 0$), the first step is virtual. Since individual steps in Raman scattering do not need to conserve energy individually, but energy must only be conserved in the overall process, the second step must also be virtual and a scattered photon is emitted with a *constant* Raman shift given by $\Delta = \omega_l - \omega_s = \omega_e$. When energy broadening is taken into account for the final state n, a resonant denominator appears as in Eq. (4). If the laser frequency is resonant with $E_{\mathrm{LL}n}$, i.e., $\Omega_{nN} = 0$, the two energy denominators are simultaneously resonant at $\Delta = \omega_e$. Upon detuning of the excitation, *in addition* to the above described process another one can be conceived in which a *real* state in the broadened tail of n is excited and recombination occurs from the *real* state p. Thus, instead of the original single peak, a doublet may appear.

We recall that Eq. (4) was derived assuming Landau-number-nonconserving interband magneto-optical transitions between confined valence and electron Landau levels which, for $\Delta n = \pm 1$, are expected to be small. We discuss now a model which actually lifts the problem of Landau-number conservation in electronic Raman processes, namely, by considering interface roughness scattering. Potential fluctuations due to interface roughness can scatter carriers with a change in their in-plane crystal momentum component and thus couple states with different Landau numbers.[3,4] A schematic representation of the process considered is shown in Fig. 6(a). An intermediate step is now added to the previously discussed sequence, shown in Fig. 5(a), in which elastic scattering by roughness causes a jump of the photoexcited hole in Landau level n to a lower (higher) index Landau level m for Stokes (anti-Stokes) processes. The corresponding Feynman diagram is shown in Fig. 6(b). The conservation of Landau number in the optical transitions is now taken into account.

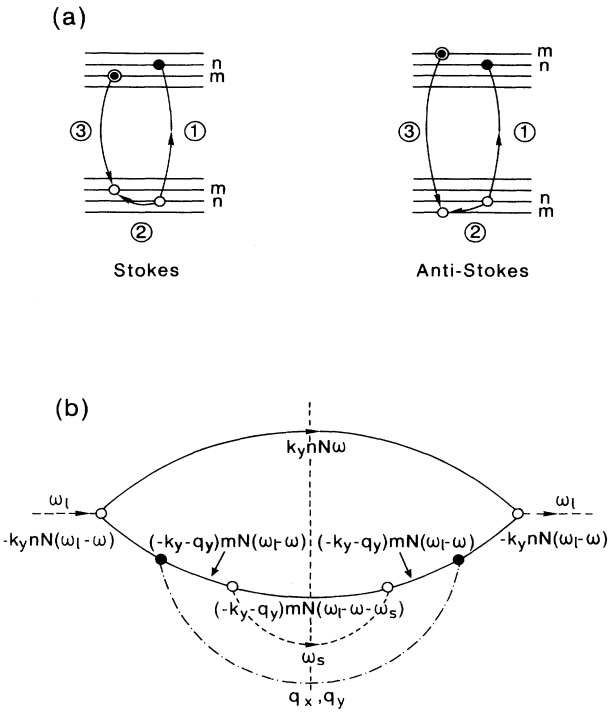

FIG. 6. (a) Schematic representation of the scattering process via single-particle inter-Landau-level electronic excitations, including elastic scattering of the hole by interface roughness. (b) Feynman-type diagram for the scattering efficiency, including the effect of interface roughness. The vertical dashed line indicates the final state in the scattering process.

Approximating the interaction of the hole with the interface roughness potential $\chi(q_\perp)$ as scattering by defects[4] and assuming an average over their in-plane positions such that translational invariance is recovered for the in-plane direction, we can sum the factors related to the hole-roughness vertex (filled circle) in the diagram of Fig. 6(b) over q_x and q_y. If the potential $\chi(q_\perp)$ is assumed to be independent of $q_\perp$[4], the sum over n and m ($m = n \pm 1$ for Stokes and anti-Stokes processes) involves only energy denominators. We obtain in this case

$$\frac{dS}{d\omega_s} \propto \sum_n \int_{-\infty}^{+\infty} \frac{d\omega}{2\pi} \gamma_{e,n}\gamma_{e,n\mp1}\{[\omega_l-\omega-E_N^h-E_g-(n\mp1+\tfrac{1}{2})\omega_h]^2+\gamma_{h,n\mp1}^2\}^{-1} \tag{6}$$
$$\times\{[\omega-E_N^e-(n+\tfrac{1}{2})\omega_e]^2+\gamma_{e,n}^2\}^{-1}\{[\omega_l-\omega-E_N^h-E_g-(n+\tfrac{1}{2})\omega_h]^2+\gamma_{h,n}^2\}^{-1}$$
$$\times\{[\omega_l-\omega-\omega_s+E_N^e+(n\mp1+\tfrac{1}{2})\omega_e]^2+\gamma_{e,n\mp1}^2\}^{-1}.$$

This expression has to be multiplied by the occupation numbers of the states involved in the scattering process: $[1-n_h^v(n)]\,[1-n_e^c(n)]\,[1-n_h^v(m)]\,n_e^c(m) \approx n_e^c(m)$. The last approximation holds when the laser-induced concentrations of electrons n_e^c and holes n_h^v are small. In our calculations, $n_e^c(n)$ was taken to be exponential in the electron energy (i.e., in m). Similar to Eq. (4), Eq. (6) can be integrated analytically. However, the expression becomes rather bulky and no new physical insight can be gained from it. We thus do not reproduce it here.

We show instead in Fig. 7 calculated Raman spectra obtained from Eq. (6) for the same magnetic field and laser frequencies as those of Fig. 3. For comparison, the calculated curves have been scaled with the same factors as the experimental ones. All parameters are given in the figure caption.

The calculated spectra reproduce the following features of the experimental results: (i) Raman peaks appear in both Stokes (SRS) and anti-Stokes (ARS) scattering, at the energy of one electron cyclotron quantum, (ii) the intensity of these peaks decays when the laser moves out of the incoming resonance with LL3, and (iii) the ratio of amplitudes between the Stokes and anti-Stokes components is reproduced using an electron temperature of $T_e \approx 60$ K, consistent with that derived from the luminescence tail in Fig. 1. In the calculated spectra of Fig. 7 other peaks appear in addition to the cyclotron resonances (SRS and ARS). They are located at absolute energies of $E_{\mathrm{LL3}} - \omega_e$, E_{LL3}, and E_{LL2} and are due to the *final state broadening effects* discussed above. The latter two resemble the luminescencelike (LLn) peaks observed in Fig. 3. We note, however, that LL2 is the *largest* structure measured in the inter-Landau-level scattering energy region of Fig. 3 and not a weak satellite like that calculated in Fig. 7. Therefore further mechanisms must contribute to LL2. We argue below that LL2 can be explained if Raman scattering by acoustic phonons is invoked.

We have also studied the dependence of the SRS and ARS peaks on excitation energy. The spectra of Fig. 3 were obtained by exciting in resonance with LL3. For excitation at higher Landau-number magneto-optical transitions, at the same applied field, we observe the SRS peak, but not its anti-Stokes counterpart ARS. This can be explained as being due to a combination of the lower electron density and the shorter lifetime of the higher-index Landau levels.

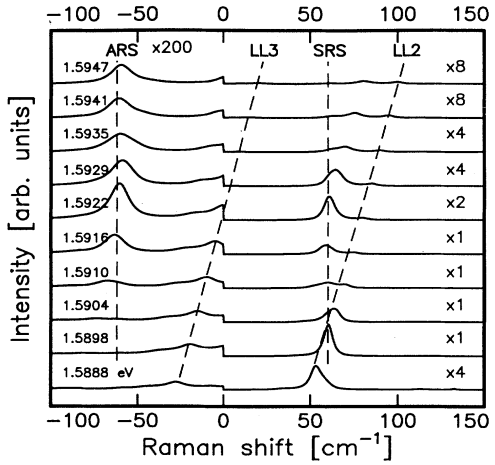

FIG. 7. Theoretical electronic Raman scattering spectra calculated for the experimental conditions of Fig. 3. For comparison, we have scaled the calculated curves with the same factors as the experimental ones. The parameters used for the calculations were $E_g = 1.5575$ eV, $H = 4.7$ T, $m_e = 0.076$, $m_h = 0.22$, $n_e \sim \exp(-n\frac{\omega_e/\omega_{\mathrm{LO}}}{0.15})$, and $T_e \approx 60$ K. All broadenings are calculated using $\Gamma_n = 0.05(n+1)^2$ meV.

Regarding the selection rules for the electron cyclotron scattering, note that in our model both single-particle scattering with and without spin flip are allowed.[1,12] The larger intensity observed for the polarized scattering reveals a spin polarization of the photoinduced carrier population. This is consistent with previous papers,[17,18] which showed that the complete quantization of the two-dimensional energy structure in large perpendicular magnetic fields makes spin-conserving relaxation processes in both thermalization and recombination much faster than spin-flip processes.

Finally, we would like to comment on the results presented in Ref. 6. We conjecture that electronic inter-Landau-level scattering in Faraday backscattering configuration with a magnetic field applied along the MQW growth direction, which was not seen there, is observed in our study of more than three times narrower QW's due to larger effective disorder (e.g., the effect of monolayer thickness fluctuations is larger the smaller the well width). Another reason might be that our experiments are performed at interband magneto-optical transitions of the E_0 gap and the associated confined heavy-hole and electron subbands, whereas those reported in Ref. 6 used the resonant enhancement of the electronic Raman efficiency at $E_0 + \Delta_0$.

B. Acoustic-phonon scattering

We have demonstrated in the preceding subsection that the Raman features SRS and ARS in Fig. 3 can be explained as being due to disorder-induced electronic scattering processes. We now turn our attention to the luminescencelike peak discussed in Sec. II (LL2 in Fig. 3). As mentioned before, (i) the energy position of this peak coincides with a magneto-optical interband transition, (ii) the feature is not observed in crossed polarizations, (iii) its intensity is linear with excitation power, (iv) it shows double-resonance behavior, and (v) it is much stronger than the corresponding features shown in the calculations of Fig. 7. Extending the theory developed for the continuous emission background in Refs. 2 and 4, we attribute the LL2 peak to Raman scattering involving acoustic phonons. In the following we analyze qualitatively three possible scattering processes: (i) third-order scattering with one-phonon emission, (ii) a fourth-order process of one-phonon and interface roughness scattering, and (iii) a process with the emission of two phonons.

The simplest possible mechanism responsible for the observed scattering would be one-acoustic-phonon emission [process (i)].[2,4] Layer thickness fluctuations cause a partial breakdown of crystal momentum conservation along the growth axis and correspondingly acoustic phonons from the whole Brillouin zone contribute to Raman scattering.[2,4] While this mechanism causes a pronounced background near the exciting laser line, the scattering intensity is strongly suppressed for the large Raman shifts Δ considered here due to the oscillatory $(\sin\Delta/\Delta)$-like behavior of the electron-phonon matrix element.[19] Due to the zero value of the in-plane com-

ponent of crystal momentum transfered to the phonon in backscattering geometry, the Landau numbers of the incoming and outgoing channels should be the same. Hence, despite the almost doubly resonant enhancement of continuous emission for $\Omega_{nN} \approx 0$ and Δ smaller than the homogeneous linewidth, no double resonances comparable to those observed here can arise from this mechanism.

We have analyzed the possibility of generating double resonances by considering interface-roughness-mediated one-phonon scattering [process (ii)]. An electron can change its Landau number after the emission of a phonon with in-plane crystal momentum $q_\perp \neq 0$. The conservation of n (or similarly of $q_\perp$) in the interaction with light can be retained if an in-plane potential, such as that due to interface roughness, scatters the hole in the intermediate state. A scattering mechanism can hence be conceived, in which an electron-hole pair is created in LL(n+1) and, after emission of an acoustic phonon by the electron and roughness scattering of the hole, recombines from LLn.

However, this mechanism also does *not* lead to double resonances. A careful evaluation of its contribution to the Raman efficiency including the two possible processes with phonon and roughness scattering, one where the first interaction is with a phonon, the other where the time sequence is inverted so that the first interaction is with the roughness potential, shows that there is a compensating effect and that the double resonance cancels.

Double and triple resonances are possible in fourth-order Raman scattering via two-phonon emission [process (iii)].[20,21] The observation of these processes involving optical phonons in GaAs was reported in Ref. 21, where a sample was uniaxially compressed in order to obtain the heavy-hole–light-hole splitting necessary for double or triple resonance. Here we consider the limit in which layer thickness fluctuations cause scattering from *single quantum wells* and thus nonconservation of crystal momentum along z. Hence a *continuous* spectrum of acoustic phonons can be tuned to resonance with the electron and hole cyclotron energies.

Evaluation of the fourth-order Raman efficiency for scattering from a single QW in a process where the electron and the hole emit phonons $\omega_{\rm ph1}$ and $\omega_{\rm ph2}$, respectively, leads to

$$\frac{dS}{d\omega_s} \propto \int_0^\infty dx \int dq_z d\tilde{q}_z \delta(\Delta - \omega_{\rm ph1}(q_z,x) - \omega_{\rm ph2}(\tilde{q}_z,x)) \times \left| \sum_{n,m} f_{nm}^2(x) \Upsilon(q_z)\Upsilon(\tilde{q}_z) \left[\frac{1}{\Omega_{nN}(\Omega_{mN}-\Delta)} \left(\frac{1}{[\Omega_{nN} + (n-m)\omega_e - \omega_{\rm ph1}(q_z,x)]} + \frac{1}{[\Omega_{nN} + (n-m)\omega_h - \omega_{\rm ph2}(\tilde{q}_z,x)]} \right) \right] \right|^2, \quad (7)$$

where $x = l_H^2 q_\perp^2/2$ and $q_\perp$ is the absolute value of the in-plane component of the phonon wave vector which is conserved, i.e., it has the same magnitude but opposite sign for the two phonons. $\Upsilon(q_z)$ is the electron-phonon matrix element of Ref. 2. To simplify the equation, we did not explicitly write down the corresponding broadenings for intermediate electron and hole states. The two terms in large square brackets differ by the sequence of phonon emission. According to Eq. (7), a resonance exists whenever $\Delta = \Omega_{mN}$, that is, a peak should appear at LLm, as observed in the experiments. This condition for outgoing resonance can always be fullfiled as long as there are two phonons in the acoustic branch with energies large enough to satisfy energy conservation. An interesting point of Eq. (7) is that the resonance conditions for both incoming $\Omega_{nN} = 0$ and outgoing $\Omega_{mN} - \Delta = 0$ channels together do not lead to double resonance since the sum of the two terms in large square brackets becomes small

$$\frac{1}{[\Omega_{nN} + (n-m)\omega_e - \omega_{\rm ph1}(q_z,x) + i\Gamma]} + \frac{1}{[\Omega_{nN} + (n-m)\omega_h - \omega_{\rm ph2}(\tilde{q}_z,x) + i\Gamma]} = -\frac{2i\Gamma}{[(n-m)\omega_e - \omega_{\rm ph1}]^2 + \Gamma^2}. \quad (8)$$

If we assume that the state after emission of one phonon is virtual (double resonance), i.e., the denominator does not vanish, the expression of Eq. (8) is of the order of Γ. However, although the *double* resonance is not realized because of this compensation effect (similar to that for the interface-roughness-mediated one-phonon scattering discussed above), there is a possibility of *triple* resonance when, in addition to $\Omega_{Nn} = 0$ and $\Omega_{mN} - \Delta = 0$, the phonon frequencies satisfy the condition $\omega_{\rm ph1}(q_z,x) = (n-m)\omega_e$ or, equivalently, $\omega_{\rm ph2}(\tilde{q}_z,x) = (n-m)\omega_h$. The value of the term in Eq. (8) is then proportional to $1/\Gamma$. This can be invoked to explain the strong increase of the LLn peak for incoming resonance. The calculation of the Raman efficiency given by Eq. (7) is complicated because an additional integration over the phonon wave vectors has to be performed.

We note that the continuous emission background described in Refs. 2–4 reflects properties of the matrix elements for electron-phonon and electron-roughness interactions and is thus qualitatively similar for spectra with or without a magnetic field. On the other hand, the acoustic-phonon-related emission peaks just discussed have their origin in the resonance denominators of the discrete MQW electronic structure in a strong magnetic field.

C. The electron effective mass

The observation of electronic inter-Landau-level scattering under resonant excitation of low number magneto-optical transitions allows us to experimentally determine electron effective masses in undoped MQW's. Normally this is done in doped QW's. In *undoped* samples, electron masses are usually determined by fitting a theoretical model to fan plots obtained in interband magneto-optical experiments.[9,22,23] This is a rather indirect method since a detailed model of the valence band structure must be assumed. The electron masses have also been determined in undoped MQW's by means of optically detected cyclotron resonance experiments.[24]

The electron energies and masses in quantum wells, including corrections due to non-parabolicity, are discussed in Ref. 25. In the limit of small magnetic fields, the electron cyclotron mass, defined by the relation $m_c = \hbar eB/\Delta E(B)$, where $\Delta E(B)$ is the energy difference between two Landau levels, is equal to the in-plane mass, i.e., the mass related to the electron in-plane dispersion at the bottom of the band. Nonparabolicity effects, which become important at large magnetic fields, cause m_c to increase with increasing field and Landau level index n.[25]

The measured electron cyclotron energy (SRS in Fig. 4) is linear with the magnetic field between 3 T and 12 T. Also, different Landau-level transitions LLn are resonant over that range of fields for a fixed excitation energy. Additionally, for a fixed magnetic field we obtain the same Raman shift when exciting in resonance with different LLn transitions [61(3) cm^{-1} for $n = 3$ and 61(4) cm^{-1} for $n = 4$ at 4.7 T]. We have hence determined the in-plane electron effective mass from the slope of a linear fit of the SRS vs B curve in Fig. 4. We find a small zero field offset in the cyclotron resonance energy [2.5(1.0) cm^{-1}], as previously reported.[24] We derive an electron parallel mass $m_c = 0.076(1)$, in agreement with Ref. 25, where an enhancement of the effective electron masses in MQW's with respect to the bulk values was predicted. This mass is somewhat larger than that calculated using Ref. 25 ($m_c = 0.074$) and the one obtained from the magneto-optical study of the same sample in Ref. 9 [$m_c = 0.073(1)$]. A larger experimental effective electron mass, as compared to the predictions of Ref. 25, was also found in Ref. 23. We note, however, that $m_c = 0.074(1)$ (and thus better agreement with the calculated values) is obtained if we force the linear fit through zero offset at $B = 0$.

IV. CONCLUSIONS

We have performed Raman scattering experiments in undoped MQW's at high magnetic fields, using resonant excitation at low-index magneto-optical interband transitions. We have observed two types of peaks. One is shifted from the laser frequency by the electron cyclotron energy and thus corresponds to electronic Raman scattering between conduction Landau-levels. This peak is unexpected for Landau-number-conserving electron-photon interaction processes. A theory of photoexcited electronic Raman scattering including interface roughness scattering is therefore invoked to account for its observation. Another observed peak coincides with magneto-optical transitions between hole and electron Landau levels and is believed to involve acoustic-phonon emission. We have qualitatively discussed possible mechanisms for this acoustic-phonon scattering and shown that, due to nonconservation of crystal momentum along z, triple resonance can exist for two acoustic-phonon Raman scattering processes. We have also shown that Raman scattering enables one to measure cyclotron resonance transitions and thus to determine in-plane electron effective masses even in undoped quantum wells.

ACKNOWLEDGMENTS

Two of us (A. F. and V. I. B.) acknowledge support from the Alexander von Humboldt Foundation and the European Union, respectively. We thank C. Tralleo-Giner and V. F. Sapega for several enlightening discussions. Thanks are also due to H. Hirt, M. Siemers, and P. Wurster for technical help and to F. Hamdani for a critical reading of the manuscript. This work has been partially supported by DGICYT Grant No. PB92-1076.

[1] B. Jusserand and M. Cardona, in *Light Scattering in Solids V*, edited by M. Cardona and G. Güntherodt (Springer, Heidelberg, 1989); A. Pinczuk and G. Abstreiter, *ibid.*

[2] V. F. Sapega, V. I. Belitsky, T. Ruf, H. D. Fuchs, M. Cardona, and K. Ploog, Phys. Rev. B **46**, 16 005 (1992).

[3] T. Ruf, V. I. Belitsky, J. Spitzer, V. F. Sapega, M. Cardona, and K. Ploog, Phys. Rev. Lett. **71**, 3035 (1993).

[4] V. I. Belitsky, T. Ruf, J. Spitzer, and M. Cardona, Phys. Rev. B **49**, 8263 (1994).

[5] J. M. Worlock, A. Pinczuk, Z. J. Tien, C. H. Perry, H. Störmer, R. Dingle, A. C. Gossard, W. Wiegmann, and R. L. Aggarwal, Solid State Commun. **40**, 867 (1981).

[6] R. Borroff, R. Merlin, J. Pamulapati, P. K. Bhattacharya, and C. Tejedor, Phys. Rev. B **43**, 2081 (1991).

[7] F. Iikawa, T. Ruf, and M. Cardona, Phys. Rev. B **43**, 4849 (1991).

[8] J. C. Maan, M. Potemski, and Y. Y. Wang, in *High Magnetic Fields in Semiconductor Physics II*, edited by G. Landwehr, Springer Series of Solid State Science Vol. 87 (Springer-Verlag, Berlin, 1988), p. 248.

[9] G. Goldoni, T. Ruf, V. F. Sapega, A. Fainstein, and M. Cardona (unpublished).

[10] J. Shah, IEEE J. Quantum Electron. **22**, 1728 (1986).

[11] S. I. Gubarev, T. Ruf, M. Cardona, and K. Ploog, Phys. Rev. B **48**, 1647 (1993).

[12] E. Burstein, A. Pinczuk, and D. L. Mills, Surf. Sci. **98**, 451 (1980).

[13] E. L. Ivchenko, I. G. Lang, and S. T. Pavlov, Fiz. Tverd. Tela (Leningrad) **19**, 2751 (1977) [Sov. Phys. Solid State **19**, 1610 (1977)].

[14] A. V. Goltsev, I. G. Lang, S. T. Pavlov, and M. F. Bryzhina, J. Phys. C **16**, 4221 (1983).

[15] V. I. Belitsky, M. Cardona, I. G. Lang, and S. T. Pavlov, Phys. Rev. B **46**, 15 767 (1992).
[16] V. I. Belitsky, A. Cantarero, and S. T. Pavlov (unpublished).
[17] M. Potemski, J. C. Maan, A. Fasolino, K. Ploog, and G. Weimann, Phys. Rev. Lett. **63**, 2409 (1989).
[18] J. B. Stark, W. H. Knox, and D. S. Chemla, Phys. Rev. Lett. **68**, 3080 (1992).
[19] T. Ruf, J. Spitzer, V. F. Sapega, V. I. Belitsky, M. Cardona, and K. Ploog, Phys. Rev. B **50**, 1792 (1994).
[20] R. M. Martin and L. M. Falicov, in *Light Scattering in Solids I*, edited by M. Cardona and G. Güntherodt (Springer, Heidelberg, 1983).
[21] A. Alexandrou, C. Trallero-Giner, G. Kanellis, and M. Cardona, Phys. Rev. B **40**, 1013 (1989).
[22] F. Ancilotto, A. Fasolino, and J. C. Maan, Phys. Rev. B **38**, 1788 (1988).
[23] A. Cros, T. Ruf, J. Spitzer, M. Cardona, and A. Cantarero, Phys. Rev. B **50**, 2325 (1994).
[24] R. J. Warburton, J. G. Michels, R. J. Nicholas, J. J. Harris, and C. T. Foxon, Phys. Rev. B **46**, 13 394 (1992).
[25] U. Ekenberg, Phys. Rev. B **40**, 7714 (1989).